



This is a repository copy of *Selective harmonic generation for dielectric barrier discharge reactors*.

White Rose Research Online URL for this paper:
<https://eprints.whiterose.ac.uk/id/eprint/227545/>

Version: Accepted Version

Proceedings Paper:

O’Keeffe, H., Foster, M.P. orcid.org/0000-0002-8565-0541 and Davidson, J.N. orcid.org/0000-0002-6576-3995 (2024) Selective harmonic generation for dielectric barrier discharge reactors. In: IET Conference Proceedings. 13th International Conference on Power Electronics, Machines and Drives (PEMD 2024), 10-13 Jun 2025, Nottingham, United Kingdom. Institution of Engineering and Technology (IET) , pp. 576-581.

<https://doi.org/10.1049/icp.2024.2210>

© 2024 The Authors. Except as otherwise noted, this author-accepted version of a journal article published in 13th International Conference on Power Electronics, Machines and Drives (PEMD 2024) is made available via the University of Sheffield Research Publications and Copyright Policy under the terms of the Creative Commons Attribution 4.0 International License (CC-BY 4.0), which permits unrestricted use, distribution and reproduction in any medium, provided the original work is properly cited. To view a copy of this licence, visit <http://creativecommons.org/licenses/by/4.0/>

Reuse

This article is distributed under the terms of the Creative Commons Attribution (CC BY) licence. This licence allows you to distribute, remix, tweak, and build upon the work, even commercially, as long as you credit the authors for the original work. More information and the full terms of the licence here:
<https://creativecommons.org/licenses/>

Takedown

If you consider content in White Rose Research Online to be in breach of UK law, please notify us by emailing eprints@whiterose.ac.uk including the URL of the record and the reason for the withdrawal request.



eprints@whiterose.ac.uk
<https://eprints.whiterose.ac.uk/>

SELECTIVE HARMONIC GENERATION FOR DIELECTRIC BARRIER DISCHARGE REACTORS

Henry O’Keeffe^{1*}, Martin P Foster¹, Jonathan N Davidson¹

¹Dept. of Electrical and Electronic Engineering, University of Sheffield, Sheffield United Kingdom

*hokeeffe1@sheffield.ac.uk

Keywords: DC-AC Converter, Power Supply, Plasma, Waveform Generator

Abstract

This paper presents a high voltage waveform generator capable of generating waveforms composed of multiple sinewaves whose frequencies are integer multiples of a fundamental frequency (harmonics). The proposed approach allows synthesis of inverter pulse-trains with a large number of controlled harmonics, called selective harmonic generation. These waveforms are produced with a GaN inverter and tested for their utility in generating ozone in a dielectric barrier discharge reactor, obtaining 193 ppm/W (parts per million per watt) with a 0.5 lpm (litre per minute) flowrate of dry air as the feedstock.

1 Introduction

1.1 Dielectric Barrier Discharge Reactors

Dielectric barrier discharge (DBD) reactors are used in a myriad of applications, including efficient generation of ozone with oxygen or air as the feedstock [1], the destruction of unwanted chemicals [2] or biological materials [3] and the production of high-value chemicals. In some reactors this is done directly, for example ozone is often produced from air or oxygen using just the reactor, whilst other reactors may use an intermediate gas to carry energetic chemical species to another chemical where further reactions occur.

50 Hz, at 10 kV_{pk}. Most DBD reactors in the literature use sinusoidal waveforms [5], but others have experimented with pulsed sinusoids [6], triangle waves, and square waves [7].

This work explores the development of a power supply intended to evaluate the performance of an ozone producing DBD reactor with a waveform consisting of two sinusoidal components, a first and second harmonic.

1.2 Selective Harmonic Elimination and Generation

Patel and Hoft introduced a technique to eliminate unwanted harmonics in an inverter pulse-train in 1973 [8]. This method involves estimating a possible solution for switching angles that may generate the required fundamental waveform with low harmonic content, then using Newton’s method to improve this guess. They were able to zero 5th, 7th, 11th, 13th and 17th harmonics in a 3-level inverter with a frequency modulation ratio of 10 pulses per fundamental cycle.

Due to improvements in computational technology, far more harmonics can now be zeroed using this method, and even extended to multi-level inverters [9]. This technique can also be applied to generate pulse-trains with any desired harmonic content, turning selective harmonic elimination (SHE) into selective harmonic generation (SHG).

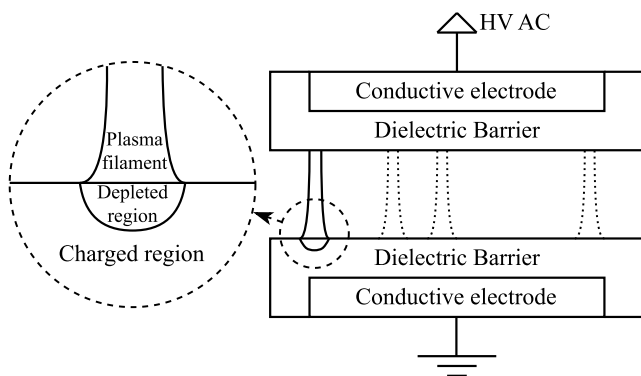


Fig. 1 Operation of a DBD reactor

DBD reactors usually consist of a pair of electrodes with one or more dielectric barrier layers and a gap for gas to pass through. As a high-voltage (HV) AC waveform is applied to the electrodes, the gas undergoes dielectric break-down as the local charge built up on the surface of the dielectric discharges in thin filaments (Fig 1).

DBD reactors are powered by high voltage AC waveforms with widely varying parameters depending on the application and design of the reactor; for example, a low power (12 W) reactor might use a 25 kHz, 5 kV_{pk} AC supply [4], whilst the largest reactors used for waste water treatment might require

2 Design

2.1 DBD Reactor Design

The reactor used in this system is designed to produce ozone using dry air as the feedstock. The reactor can be seen in Fig. 2. The gas enters the reactor from the rear, passing through a set of small holes, directing the gas to the reaction gap. It then travels around the upper electrode and exits through the top the reactor. The upper electrode with electrical connection **A** is aluminium, whilst the lower electrode with connection **B** is aluminium with a dielectric layer of alumina (aluminium oxide) surrounding it. The output of the reactor can be connected to an ozone monitor to quantify the output of the reactor. Specifications for this reactor can be found in Table 1.

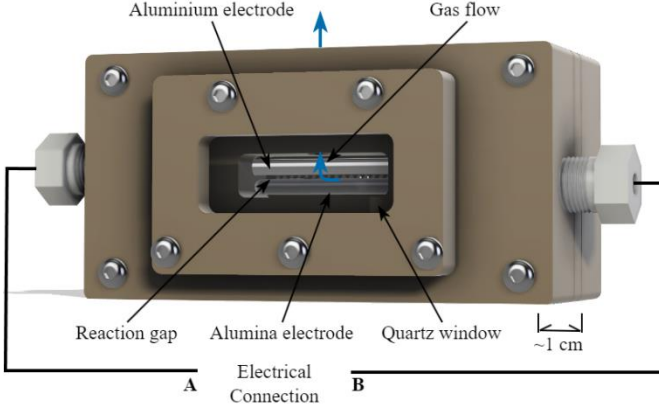


Fig. 2 DBD reactor structure

Table 1 Reactor Specifications

Electrode diameter	3 mm
Alumina dielectric thickness	0.675 mm
Average electrode gap distance	~0.25 mm
Electrode active length	20 mm
Flowrate	0.5 lpm
Maximum reactor voltage	5 kV _{pk}

2.2 Selective Harmonic Generation Algorithm

Fig. 3 shows an example inverter waveform with 6 pulses per cycle with each pulse labelled 1-6. The terminology ϕ_{Sa} to represent the start of pulse a , and ϕ_{Ea} to represent the end of pulse a such that the duration of pulse 1 is $\phi_{E1} - \phi_{S1}$.

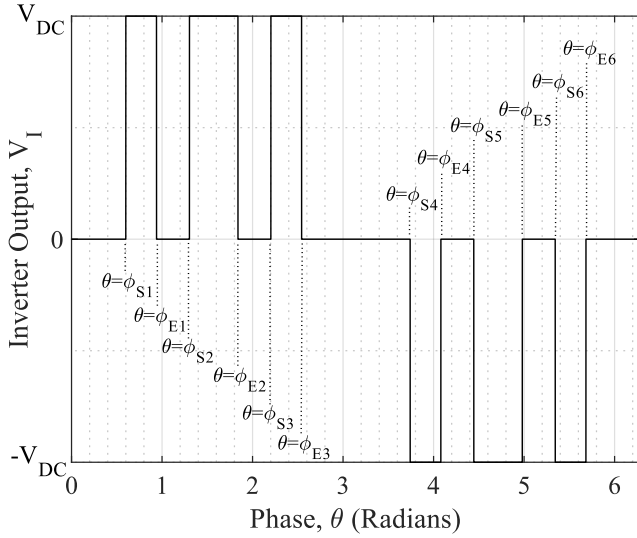


Fig. 3 Example pulse-train waveform

During the interval $\phi_{Sa} < \theta < \phi_{Ea}$ and $\theta < \pi$, Sw_1 and Sw_4 (shown in Fig. 4) are on and $V_I = V_{DC}$. When $\phi_{Sa} < \theta < \phi_{Ea}$ and $\theta \geq \pi$, Sw_2 and Sw_3 are on and $V_I = -V_{DC}$. Otherwise, Sw_3 and Sw_4 are on, and $V_I = 0$. There are always an even number of pulses per cycle, and if the modulated waveform is dominated by a fundamental frequency with a period, $\theta = 2\pi$, switching angles above π will result in a negative voltage, as in Fig. 3.

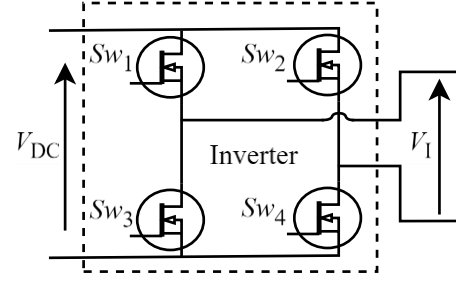


Fig. 4 Inverter circuit diagram

Both SHE and SHG are based on the Fourier-series expansion of a bipolar pulse-train, similar to that shown in Fig. 3. The sine-cosine form of the Fourier series is,

$$f(\theta) = A_0 + \sum_{n=1}^{\infty} (A_n \cos(n\theta) + B_n \sin(n\theta)) \quad (1)$$

where,

$$A_0 = \frac{1}{2\pi} \int_0^{2\pi} s(\theta) d\theta \quad (2)$$

$$A_n = \frac{1}{\pi} \int_0^{2\pi} s(\theta) \cos(n\theta) d\theta \quad (3)$$

$$B_n = \frac{1}{\pi} \int_0^{2\pi} s(\theta) \sin(n\theta) d\theta \quad (4)$$

The waveform function is s , and is given by,

$$s(\theta) = \begin{cases} V_{DC}, & \phi_{S1,2,3\dots} < \theta < \phi_{E1,2,3\dots} \text{ and } \theta < \pi \\ -V_{DC}, & \phi_{S1,2,3\dots} < \theta < \phi_{E1,2,3\dots} \text{ and } \theta \geq \pi \\ 0, & \text{otherwise} \end{cases} \quad (5)$$

Equation (5) can be substituted into (3) and the integration evaluated to give,

$$A_n = \frac{1}{n\pi} \left(\sum_{a=1}^{\frac{N_p}{2}} (\sin(n\phi_{Ea}) - \sin(n\phi_{Sa})) - \sum_{a=\frac{N_p}{2}+1}^{N_p} (\sin(n\phi_{Ea}) - \sin(n\phi_{Sa})) \right) \quad (6)$$

where N_p is the number of pulses per cycle. Similarly,

$$B_n = \frac{1}{n\pi} \left(\sum_{a=1}^{\frac{N_p}{2}} (\cos(n\phi_{Sa}) - \cos(n\phi_{Ea})) - \sum_{a=\frac{N_p}{2}+1}^{N_p} (\cos(n\phi_{Sa}) - \cos(n\phi_{Ea})) \right) \quad (7)$$

By ensuring half-wave symmetry, (2) and (6) evaluate to $A_0 = 0$, $A_n = 0$ [8].

To determine the required switching angles to generate the desired harmonics $B_{1,2,3,\dots}$ (7) can be represented as a system of equations, $G(\phi)$, where ϕ represents the switching angles:

$$\begin{aligned} \cos(\phi_{S1}) - \cos(\phi_{E1}) + \cos(\phi_{S2}) - \cos(\phi_{E2}) \dots - \pi B_1 &= 0 \\ \cos(2\phi_{S1}) - \cos(2\phi_{E1}) + \cos(2\phi_{S2}) - \cos(2\phi_{E2}) \dots - 2\pi B_2 &= 0 \\ \cos(3\phi_{S1}) - \cos(3\phi_{E1}) + \cos(3\phi_{S2}) - \cos(3\phi_{E2}) \dots - 3\pi B_3 &= 0 \\ &\vdots \end{aligned} \quad (8)$$

The switching angles for the negative half of the waveform are mirrored about $\theta = \pi$,

$$\begin{aligned} \phi_{E2N_p} &= 2\pi - \phi_{S1} \\ \phi_{S2N_p} &= 2\pi - \phi_{E1} \\ \phi_{E2N_p-1} &= 2\pi - \phi_{S2} \\ \phi_{S2N_p-1} &= 2\pi - \phi_{E2} \\ &\vdots \end{aligned} \quad (9)$$

The system in (8) has N_p equations in N_p unknowns (the switching angles). This system is not linear, but can be solved numerically using Newton's method,

$$\phi_{m+1} = \phi_m - G(\phi_m) \times \left(\frac{\partial G(\phi_m)}{\partial \phi_m} \right)^{-1} \quad (10)$$

where m is the Newton iteration.

The initial conditions, ϕ_0 , were estimated by pulse-width modulating a time-domain representation of the waveform to be generated.

To ensure that the harmonics converged closely to the desired values, 15 iterations of Newton's method were carried out using 64-bit floating point maths.

For these experiments, only 1st and 2nd harmonics were required, and all the other controllable harmonics (B_n where $3 \leq n \leq N_p$) were set to 0. B_1 and B_2 were altered to adjust the amplitude of the first and second harmonic amplitude

respectively. To ensure dominance of the fundamental harmonic and keep (5) valid for the modulated waveform, $2B_2 \leq B_1$.

3 Experimental Setup

The physical system consists of a GaN H-Bridge inverter seen in Fig. 4 driving a HV transformer, connected via a current-sense capacitor to the reactor. The electrical set-up diagram can be seen in Fig. 5 and the inverter specifications in Table 2. The reactor used is shown in Fig. 2. The ozone output was measured with a 2B Technologies 106 ozone monitor.

Table 2 Inverter Specifications

Bus voltage	48 V
GaN switches	TI LMG5200
Controller IC	dsPIC33CH512MP505
Switch on-state resistance	15 m Ω
Switch slew-rate	50 V/ns
Switch current rating	10 A
PCB dimensions	55 mm \times 32 mm

The frequency response of the transformer is shown in Fig. 6. It shows a peak gain due to resonance at 80 kHz, before rolling off at approximately 40 dB/decade. To obtain high gain at the second harmonic, a fundamental frequency of 35 kHz for all tests was chosen.

$N_p = 10$, allowing the uncontrolled higher harmonics to be attenuated by approximately 30 dB compared to the gain at the fundamental frequency.

Power to the reactor was measured using the Lissajous technique [5], using a current sense capacitor, C_s (shown in Fig. 5) and equation (11).

$$P_{av} = \frac{C_s}{T_{av}} \int_{t=0}^{t=T_{av}} V_R(t) dV_{CS}(t) \quad (11)$$

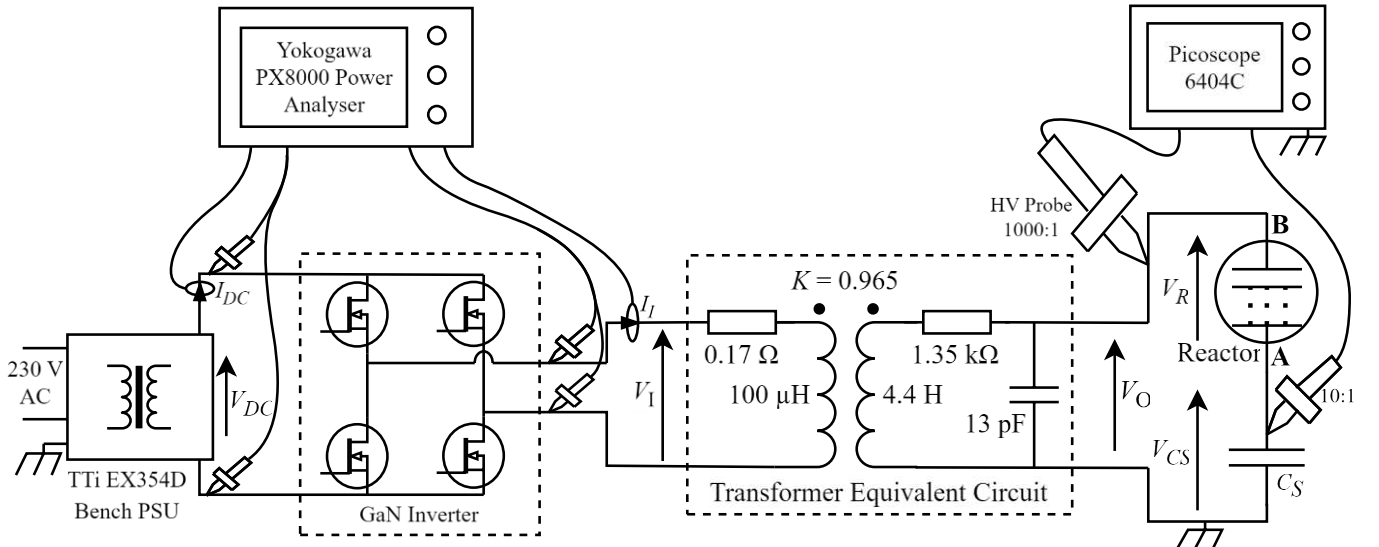


Fig. 5 Experimental setup

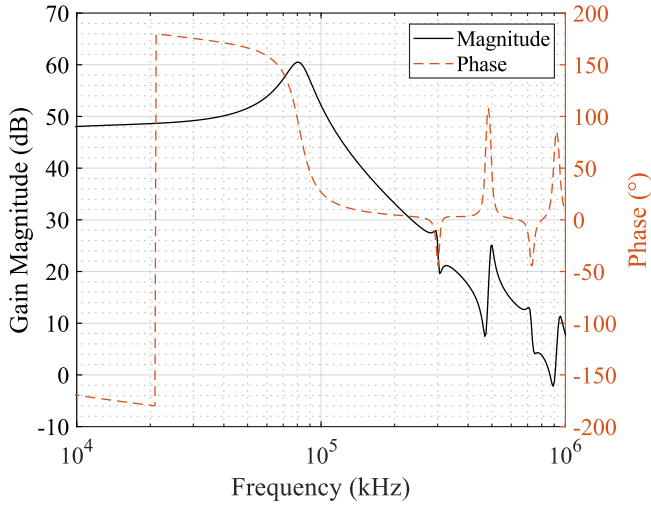


Fig. 6 Transformer frequency response

4 Experimental Results

For these tests, B_1 was adjusted from 0.114 to 0.228 and B_2 between 0 and 0.114, whilst ensuring $2B_2 \leq B_1$. It should be noted that the output of the inverter is scaled to V_{DC} so when $B_1 = 1$, $B_2 = 0$, $V_{I\text{pk}} = V_{DC}$ where $V_{I\text{pk}}$ is the magnitude of inverter output voltage for the controlled harmonics.

Fig. 7 shows the inverter output current and voltage with no second harmonic. The pulses can clearly be seen extending to ± 48 V. The 350 kHz sine wave contribution is due to switching frequency exciting the step-up transformer.

Fig. 8 shows the waveforms when the second harmonic is set to 50% of the 1st harmonic. The second harmonic is visible in the current waveform as well as the high-frequency ripple.

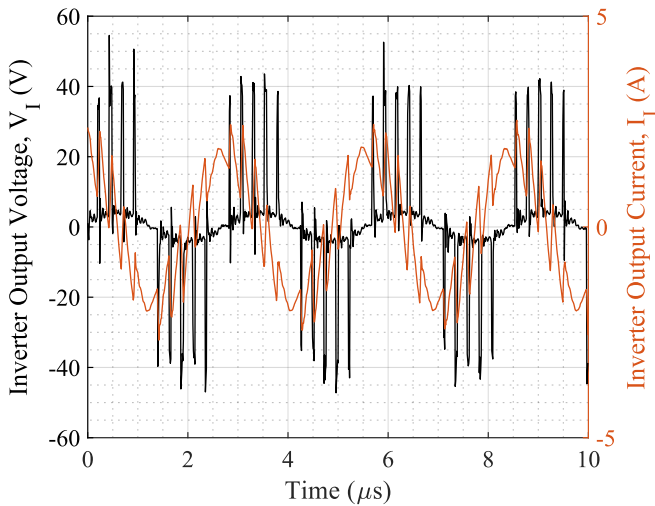


Fig. 7 Inverter output voltage V_I and current I_I when $B_1 = 0.23$, $B_2 = 0$

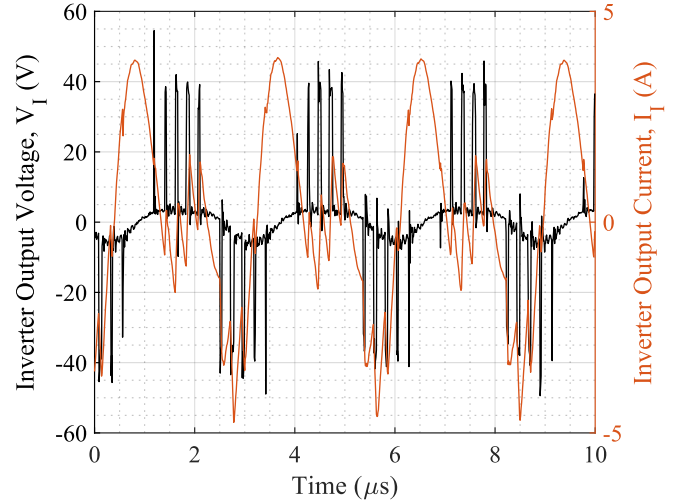


Fig. 8 Inverter output voltage V_I and current I_I when $B_1 = 0.23$, $B_2 = 0.115$

Fig. 9 and Fig. 10 show the reactor waveforms for the same conditions as in Fig. 7 and Fig. 8. The transformer has filtered out the high-frequency harmonics, leaving the waveforms closer to the desired pure 1st and 2nd harmonics.

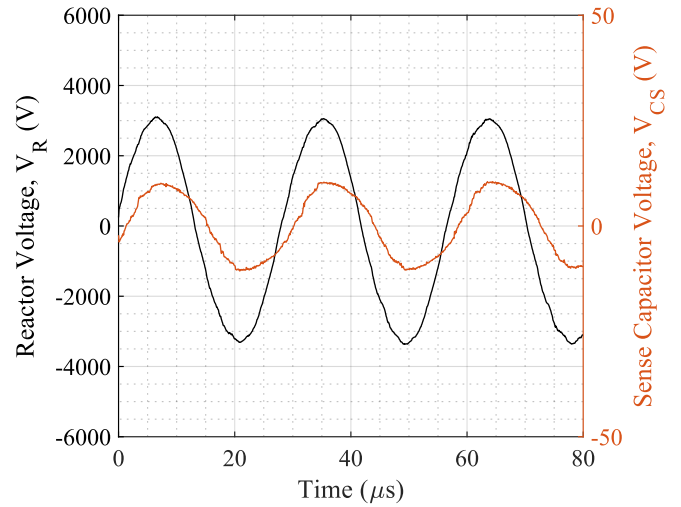


Fig. 9 Reactor voltage V_R and current sense capacitor voltage V_{CS} when $B_1 = 0.23$, $B_2 = 0$

The spectral content of the transformer output voltage is shown in Fig. 11. Harmonics above the second are attenuated by over 20 dB compared to the fundamental. When $B_2 = 0$, the uncontrolled second harmonic (V_{O2}) is 80 V_{pk} compared to the fundamental 3.2 kV_{pk} . When $B_2 = 0.115$, $V_{O2} = 1.3 kV_{\text{pk}}$, less than the 1.6 kV_{pk} predicted by difference between B_1 and B_2 . This could be due to the increased RMS voltage increasing the power in the reactor, increasing the current and the voltage drop across parasitic components in the transformer.

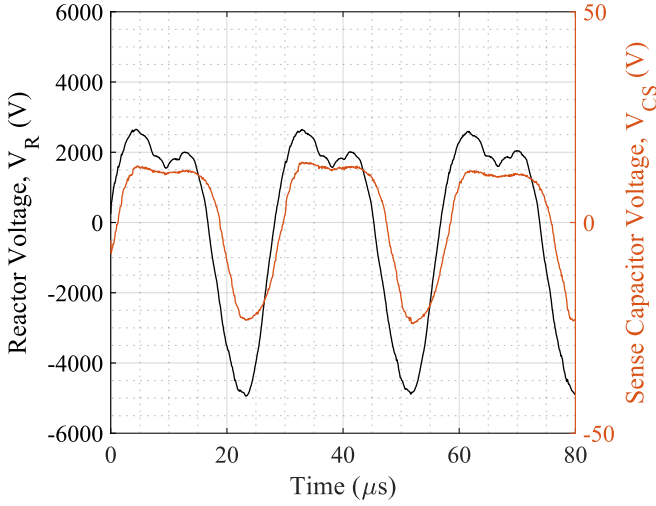


Fig. 10 Reactor voltage V_R and current sense capacitor voltage V_{CS} when $B_1 = 0.23$, $B_2 = 0.115$

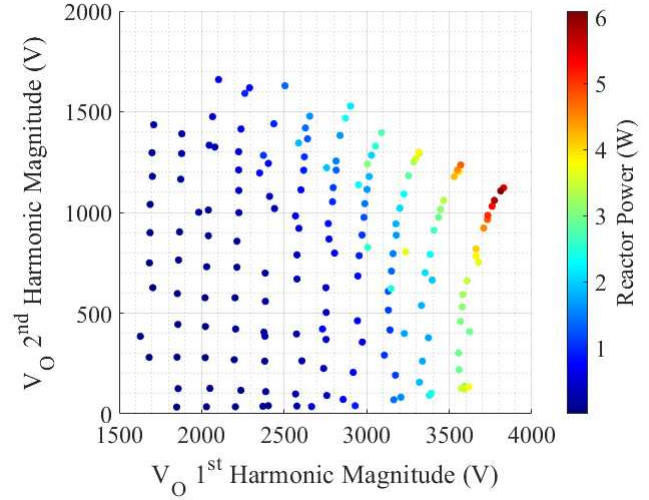


Fig. 12 Reactor power as a function of the 1st and 2nd harmonic voltage

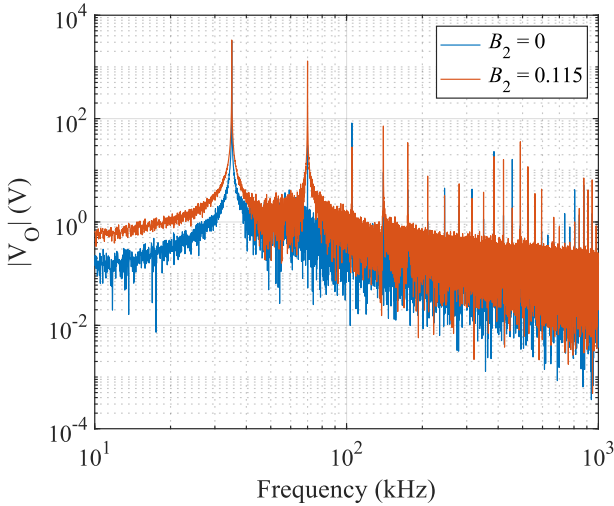


Fig. 11 Transformer output voltage ($V_{O\text{pk}}$) in the frequency domain when $B_1 = 0.23$

Fig. 12 shows power delivered to the reactor over the test-range of 1st and 2nd harmonic magnitudes. Power increased as both the magnitude of the 1st and 2nd harmonic were increased, reaching a peak of approximately 6 W. As the 1st harmonic voltage (V_{O1}) was increased and the power in the reactor increased, V_{O2} reduced, perhaps due to the increased current as discussed previously.

The ozone concentration obtained from these tests is presented in Fig. 13. The maximum ozone concentration was obtained with $V_{O1} = 3 \text{ kV}_{\text{pk}}$ and $V_{O2} = 1.25 \text{ kV}_{\text{pk}}$, at 175 ppm (parts per million).

The ozone concentration increases as both harmonic voltages are increased, then decreases sharply when $V_{O1} > 3.5 \text{ kV}_{\text{pk}}$ and $V_{O2} > 750 \text{ V}_{\text{pk}}$. This thought to be due to heating in the reactor causing ozone to be destroyed after production as ozone is highly reactive and degrades quickly at high temperatures [10].

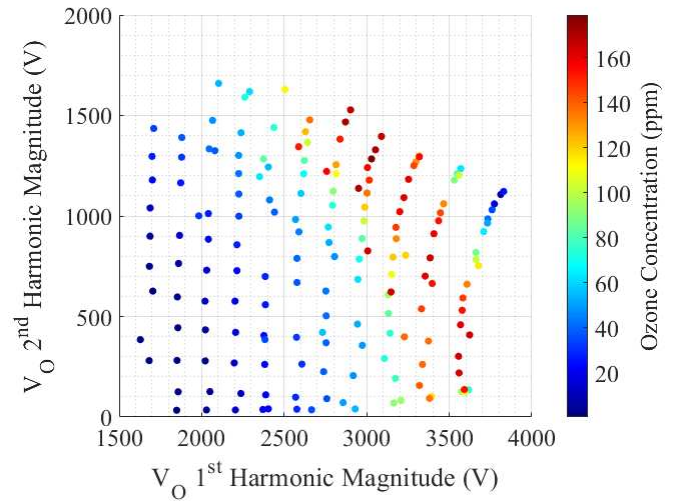


Fig. 13 Ozone concentration as a function of the 1st and 2nd harmonic voltage

Fig. 13 shows high concentrations (~150 ppm) can be obtained using $V_{O1} = 3.5 \text{ kV}_{\text{pk}}$ and $V_{O2} = 100 \text{ V}_{\text{pk}}$, by using $V_{O1} = 3 \text{ kV}_{\text{pk}}$ and $V_{O2} = 1.3 \text{ kV}_{\text{pk}}$, or some combination within this range. Fig. 14 shows that, over the same range, the reactor efficacy changes from 50 ppm/W when $V_{O2} \ll V_{O1}$ to 100 ppm/W with significant 2nd harmonic, suggesting that, in this system, efficacy can be improved by adding 2nd harmonic content to the waveform whilst slightly decreasing the fundamental amplitude.

Fig. 14 shows the efficacy of the reactor (a measure of the reactor performance in ppm/W) over the same tests. The efficacy peaks at relatively low voltages, around $V_{O1} = 2.25 \text{ kV}_{\text{pk}}$ and $V_{O2} = 600 \text{ V}_{\text{pk}}$. When combined with the ozone concentration data from Fig. 13, this represents a trade-off between efficacy and ozone concentration; the highest efficiency can only be obtained at low concentrations.

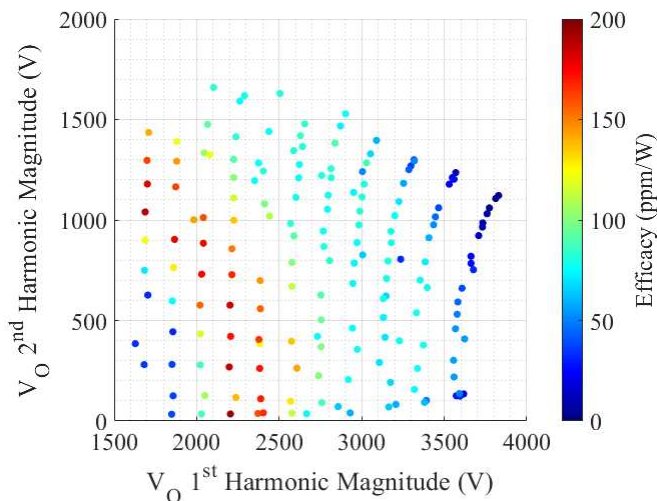


Fig. 14 Reactor efficacy as a function of the 1st and 2nd harmonic voltage

Fig. 15 shows how the transformer efficiency varies with voltage. This figure shows a similar trend to the reactor power in Fig. 12, suggesting that the transformer losses are dominated by losses associated with reactive current, rather than the load current. A better selection of transformer or operating frequency may help increase this efficiency.

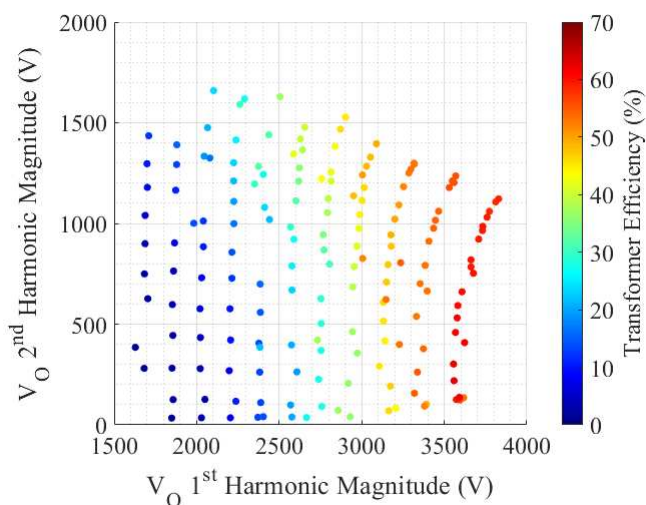


Fig. 15 Transformer efficiency as function of the 1st and 2nd harmonic voltage

5 Conclusion

In this work an approach to waveform generation based in the frequency domain has been presented. This technique, SHG, has been demonstrated to produce waveforms with harmonics close to their controlled values when used in a low voltage GaN inverter. Waveforms with a range of 1st and 2nd harmonic content have been applied to a DBD reactor, the ozone produced recorded and the effectiveness of the reactor under these conditions compared. Some additional second harmonic content was shown to increase the efficacy of the reactor when high ozone concentration (~150 ppm) is required.

6 Acknowledgements

This work has been financially supported by EPSRC: EP/S031421/1.

7 References

- [1] U. Kogelschatz, 'Dielectric-barrier Discharges: Their History, Discharge Physics, and Industrial Applications', *Plasma Chem. Plasma Process.*, vol. 23, no. 1, pp. 1–46, 2003.
- [2] X. Ma *et al.*, 'Plasma Assisted Catalytic Conversion of CO₂ and H₂O Over Ni/Al₂O₃ in a DBD Reactor', *Plasma Chem. Plasma Process.*, vol. 39, pp. 109–124, 2019.
- [3] A. Hafeez, N. Shezad, F. Javed, T. Fazal, M. S. Rehman, and F. Rehman, 'Developing multiplexed plasma micro-reactor for ozone intensification and wastewater treatment', *Chem. Eng. Process. - Process Intensif.*, vol. 162, p. 108337, 2021.
- [4] K. Nassour, M. Brahami, S. Nemnich, N. Hammadi, N. Zouzou, and A. Tilmatine, 'Comparative Experimental Study between Surface and Volume DBD Ozone Generator', *Ozone Sci. Eng.*, vol. 38, no. 1, pp. 70–76, 2016.
- [5] F. Peeters and T. Butterworth, 'Electrical Diagnostics of Dielectric Barrier Discharges', in *Atmospheric Pressure Plasma - From Diagnostics to Applications. IntechOpen*, 2018. doi: 10.5772/intechopen.80433.
- [6] T. Homola, V. Prukner, P. Hoffer, and M. Šimek, 'Multi-hollow surface dielectric barrier discharge: an ozone generator with flexible performance and supreme efficiency', *Plasma Sources Sci. Technol.*, vol. 29, no. 9, p. 95014, 2020, doi: 10.1088/1361-6595/aba987.
- [7] P. Seri *et al.*, 'Influence of the voltage waveform's shape and on-time duration on the dissolved ozone produced by a DBD bubble reactor', *Plasma Sources Sci. Technol.*, vol. 28, no. 3, p. 035001, Mar. 2019, doi: 10.1088/1361-6595/ab024f.
- [8] H. S. Patel and R. G. Hoft, 'Generalized Techniques of Harmonic Elimination and Voltage Control in Thyristor Inverters: Part I--Harmonic Elimination', *IEEE Trans. Ind. Appl.*, vol. IA-9, no. 3, pp. 310–317, May 1973, doi: 10.1109/TIA.1973.349908.
- [9] Z. Salam, Y. S. Soon, and Y. Saleem, 'On the improved computational speed and convergence of the Newton Raphson iteration method for selective harmonics elimination PWM applied to cascaded multilevel inverter with equal and non-equal DC sources', *COMPEL - Int. J. Comput. Math. Electr. Electron. Eng.*, vol. 32, no. 3, pp. 901–922, Jan. 2013, doi: 10.1108/03321641311305827.
- [10] H. Itoh, M. Taguchi, and S. Suzuki, 'Thermal decomposition of ozone at high temperature leading to ozone zero phenomena', *J. Phys. Appl. Phys.*, vol. 53, no. 18, p. 185206, 2020, doi: 10.1088/1361-6463/ab71a9.